

studies appears here.

⁶Z. Siderski, I. Pelly, and R. Gomer, *J. Chem. Phys.* **50**, 2382 (1969).

⁷A. U. MacRae, K. Müller, J. J. Lander, J. Morrison, and J. C. Phillips, *Phys. Rev. Letters* **22**, 1048 (1969). See also the additional literature discussing various assumptions and conclusions on this work. K. L. Ngai, E. N. Economou, and Morrell H. Cohen, *ibid.* **24**, 61 (1970); J. W. Gadzuk, *Phys. Rev. B* **1**, 1267 (1970); C. J. Powell, *ibid.* **1**, 4191 (1970); D. L. Fehrs, T. J. Lee, E. J. Hopkins, and R. E. Stickney, *Surface Sci.* **21**, 197 (1970).

⁸R. W. Gurney, *Phys. Rev.* **47**, 479 (1935).

⁹N. S. Rasor and C. Warner, III, *J. Appl. Phys.* **35**, 2589 (1964).

¹⁰A. J. Benett and L. M. Falicov, *Phys. Rev.* **151**, 512 (1966).

¹¹J. W. Gadzuk, *Surface Sci.* **6**, 133 (1967); **6**, 159 (1967); in *The Structure and Chemistry of Solid Surfaces*, edited by G. A. Somorjai (Wiley, New York, 1969).

¹²L. W. Swanson, A. E. Bell, C. H. Hinrichs, L. C. Crouser, and B. E. Evans, Final NASA Report, Contract No. NAS3-8910, 1967 (unpublished).

¹³H. Moesta, *Chemisorption und Ionization in Metall-Metall-Systemen* (Springer, Berlin, 1968).

¹⁴E. W. Plummer and T. N. Rhodin, *J. Chem. Phys.* **49**, 3479 (1968).

¹⁵T. B. Grimley and S. M. Walker, *Surface Sci.* **14**, 395 (1969); T. B. Grimley, *J. Vacuum Sci. Tech.* **8**, 31 (1971).

¹⁶D. M. Edwards and D. M. Newns, *Phys. Letters* **24A**, 236 (1967); D. M. Newns, *Phys. Rev.* **178**, 1123 (1969); *Phys. Rev. Letters* **25**, 1575 (1970).

¹⁷J. W. Gadzuk, *J. Phys. Chem. Solids* **30**, 2307 (1969); *Surface Sci.* **23**, 58 (1970).

¹⁸E. Gerlach, in *Molecular Processes on Solid Surfaces*

(McGraw-Hill, New York, 1969).

¹⁹D. M. Newns, *J. Chem. Phys.* **50**, 4572 (1969); *Phys. Rev. B* **1**, 3304 (1970).

²⁰J. R. Schrieffer and R. Gomer, *Surface Sci.* **25**, 315 (1971).

²¹M. Remy, *J. Chem. Phys.* **53**, 2487 (1970).

²²P. W. Anderson, *Phys. Rev.* **124**, 41 (1961); and in *Many-Body Physics*, edited by C. De Witt and R. Balian (Gordon and Breach, New York, 1969).

²³J. R. Schrieffer and D. C., Mattis, *Phys. Ref.* **140**, A1412 (1965).

²⁴B. Kjällerström, D. J. Scalapino, and J. R. Schrieffer, *Phys. Rev.* **148**, 665 (1966).

²⁵J. R. Schrieffer, *J. Appl. Phys.* **38**, 1143 (1967).

²⁶E. W. Plummer and R. D. Young, *Phys. Rev. B* **1**, 2088 (1970); J. W. Gadzuk, *ibid.* **1**, 2110 (1970); J. W. Gadzuk, E. W. Plummer, H. E. Clark, and R. D. Young, in Proceedings of the Third Materials Research Symposium, Electronic Density of States, Natl. Bur. Std., 1969 (unpublished).

²⁷J. Langer and S. J. Vosko, *J. Phys. Chem. Solids* **12**, 196 (1960).

²⁸C. B. Duke, *J. Vacuum Sci. Tech.* **6**, 152 (1969).

²⁹J. R. Smith, *Phys. Rev.* **181**, 522 (1969).

³⁰N. Lang and W. Kohn, *Phys. Rev. B* **1**, 4555 (1970); **3**, 1215 (1971).

³¹A. W. Weiss, *Phys. Rev.* **166**, 70 (1968).

³²T. Engel and R. Gomer, *J. Chem. Phys.* **52**, 1832 (1970).

³³L. Pauling, *The Nature of the Chemical Bond* (Cornell U. P., Ithaca, N. Y., 1960).

³⁴*Handbook of Chemistry and Physics* (Chemical Rubber, Cleveland, 1961).

³⁵*Handbook of Mathematical Functions*, Natl. Bur. Std., Appl. Math. Series 55 (U. S. GPO, Washington, D. C., 1965), p. 228.

Atomic Configurations in Binary Alloys

Philip C. Clapp

Ledgemont Laboratory, Kennecott Copper Corporation, Lexington, Massachusetts 02173

(Received 21 January 1971)

The complete probability distribution of nearest-neighbor configurations has been inferred for a number of cubic binary alloys from their experimentally determined short-range order parameters. The probability variation method, derived previously, was used to perform the calculations. This procedure, which is used to generate n -site probabilities from experimentally measured pair probabilities, requires the physical assumption that the configurational energy of the system can be adequately represented by pairwise interactions whose range does not exceed the diameter of the cluster. Results are presented here for β -CuZn, Cu₃Au, CuAu, Au₃Cu, Cu_{85.5}Al_{14.5}, Cu₅₂Ni₄₈, and Au₆₀Pd₄₀, and the implications for ordering (or clustering) behavior are discussed. Finally, tables of coefficients for the bcc and fcc lattice are given to enable one to carry out this type of analysis for any cubic binary system.

I. INTRODUCTION

In a previous paper¹ (hereafter referred to as I) a systematic procedure was presented for using the measured values of Warren short-range order

(SRO) parameters $\{\alpha_i\}$ in binary alloys to make a "best" prediction of the probability distribution of n -site atom configurations (where n can be 10 or more). These multisite probability distributions are potentially important for understanding nuclea-

tion processes, unraveling Mössbauer spectra, estimating the distribution of strain fields at the atomic level, or simply visualizing the configurational state of a partially ordered binary system. It also offers a powerful method for predicting the atomic configuration of equilibrium low-temperature phases from high-temperature data, even when such phases are prevented from forming for kinetic reasons.

This predictive procedure was called the probability variation method (PVM), and it can be briefly summarized. If $P_k^{(n)}$ is the probability that an n -site cluster chosen randomly in the lattice is of configuration type k , then the PVM determines the $P_k^{(n)}$ by varying them to maximize the function $I = -\sum_k P_k^{(n)} \ln P_k^{(n)}$ subject to a set of linear constraints that ensure that the composition and SRO parameters of the alloy remain fixed. The method rests upon the physical assumption that the configurational energy of the lattice depends only upon the composition and the α_i 's, and thus remains constant during the variation of the $P_k^{(n)}$'s. This is equivalent to assuming that there are no important contributions to the configurational energy from three- or more-body interactions in the crystal. The PVM can then be regarded as a technique for finding the $P_k^{(n)}$'s that maximize the entropy of a microcanonical ensemble of configurational states. It was also shown in I that this microcanonical ensemble contains many more configurational states than are possible on a real lattice. A plausibility argument was given that the maximal entropy point of the real lattice ensemble always coincided with the maximal point of the artificial ensemble used in the calculations. This mathematical assumption could not be rigorously proven but was shown to be valid for a number of cases where the exact result was previously known. At the very least the PVM yields a set of P_k 's that are consistent with the experimental data on composition and SRO of the alloy. This is a significant advantage relative to other analytical methods of determining the probability distribution (such as the Kirkwood superposition approximations) that do not satisfy such self-consistency conditions.

In the present paper we have used the PVM to determine the probability distribution of a cluster consisting of a central site and all its nearest neighbors for a number of cubic alloys. In particular we have analyzed β -CuZn, Cu₃Au, CuAu, Au₃Cu, Cu_{85.5}Al_{14.5}, Cu₅₂Ni₄₈, and Au₆₀Pd₄₀ using the available experimental SRO data for these systems. We find that the most enhanced cluster configuration relative to the perfectly random distribution for the alloys β -CuZn, Cu₃Au, and CuAu is the configuration of the perfectly ordered state in each case. The surprising result emerges in Au₃Cu that at a temperature 11% above the ordering temperature the most enhanced configuration appears to be the perfectly ordered configuration of CuAu. We shall of-

fer below several possible explanations of this result.

The Cu_{85.5}Al_{14.5} results show a strong enhancement of a tetrahedral cluster of Al atoms about a central Cu atom reminiscent of the metastable ordered bcc β phase found at the Cu₃Al composition. This supports the picture of the SRO state in this system proposed by Borie and Sparks.² It also explains why Gehlen and Cohen³ found so few of these tetrahedral clusters in a computer mapping of this system since, although the tetrahedral cluster is strongly enhanced, the volume fraction of the lattice occupied in this way is still very small.

The Cu₅₂Ni₄₈ distribution shows primarily Cu- and Ni-rich clusters but with a marked tendency to cluster on (111) planes. This agrees with the model proposed by Cohen⁴ from his computer mapping of the SRO state. Further evidence in support of the growth of Ni and Cu platelets on (111) planes is given below on the basis of the pair interactions in this alloy previously determined by Moss and Clapp.⁵

The distributions derived for the Au₆₀Pd₄₀ alloy indicate a definite tendency for this system to order but it is difficult to decide what the configuration of the hypothetical perfectly ordered state is. The equilibrium phase diagram indicates a single solid solution for all compositions so that the ordering temperature is apparently too low for the ordering reaction to ever go to completion. Lin, Spruiell, and Williams⁶ have recently suggested a particular configuration for the ordered crystal on the basis of a computer simulation of the SRO state. Our distribution partially supports their conclusion but also suggests that the real answer may be even more complicated.

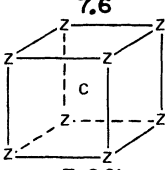
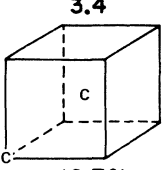
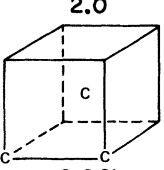
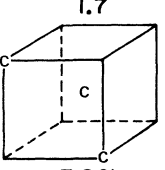
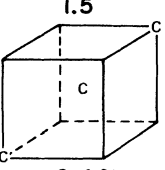
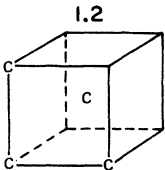
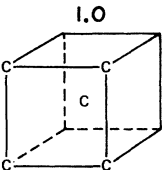
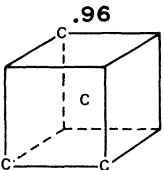
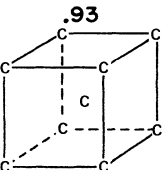
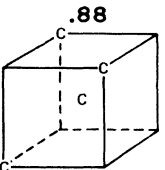
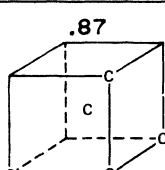
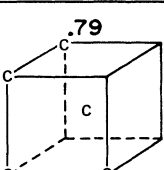
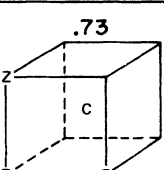
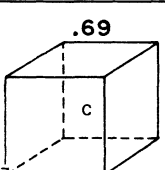
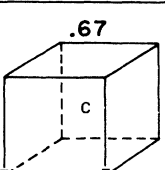
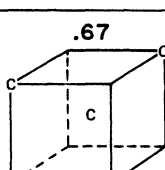
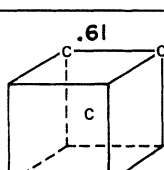
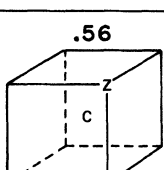
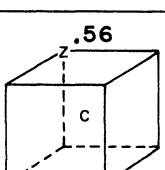
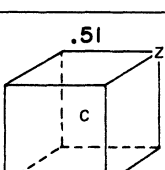
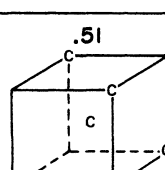
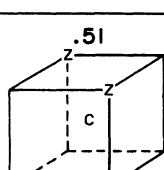
II. PROBABILITY VARIATION METHOD

The first step in applying the PVM is to choose the n -site cluster to be studied. A cluster large enough to show many details of the ordering process but small enough for the calculations to be manageable consists of a site and all of its nearest neighbors. The next step is to tabulate all of the possible configurations of this cluster and to evaluate by inspection the contribution that each configuration will make to the lattice composition and pair correlations. This was done in I for the simple example of a triplet cluster and the results were presented there in Table I. Similar tabulations for the nearest-neighbor cluster on bcc and fcc lattices are given in the Appendix. The third step is to construct the linear equations for the P_k 's where the j th equation will be of the form

$$\sum_{k=1}^K a_j^k P_k = b_j \quad (j=1, J) . \quad (1)$$

The a_j^k 's are determined from the cluster tables and the b_j 's are set by the composition and SRO

TABLE I. Nearest-neighbor spectrum of Cu atoms in CuZn at $T=543^\circ\text{C}$ ($T/T_c=1.10$).

CuZn $T = 543^\circ\text{C}$ ($T/T_c = 1.10$)				
$a_{111} = -.179$ $a_{200} = +.103$ $a_{220} = +.066$ $a_{222} = +.045$				
 7.6 3.0%	 3.4 10.7%	 2.0 9.2%	 1.7 7.8%	 1.5 2.4%
 1.2 11.8%	 1.0 2.4%	 .96 8.9%	 .93 .4%	 .88 2.7%
 .87 2.7%	 .79 7.4%	 .73 6.7%	 .69 2.2%	 .67 3.1%
 .67 6.2%	 .61 1.4%	 .56 2.6%	 .56 5.3%	 .51 .80%
 .51 .4%	 .51 1.6%			
TOTAL 100%				

data. These equations are also contained in the Appendix.

The number of linear equations J is always exceeded by K , the number of unknowns (the P_k 's); with additional conditions that each P_k must not be less than zero, the possible range of each P_k may be quite small. In fact, if the pair correlations are assigned the values corresponding to a perfectly ordered structure, the P_k 's will become completely determined.

So far no approximations have been introduced, and any set of P_k 's that satisfies the above conditions

would represent a possible state of the lattice. If the P_k 's are sufficiently limited by these conditions, it may not be necessary to go further. However, when the lattice contains a substantial degree of disorder, it is desirable to determine the most probable set of P_k 's. It was pointed out in I that this most probable set will represent the state of the lattice all but a negligible fraction of the time.

It is impossible to proceed further by any method without making some assumption about the configurational energy of the lattice. The basic hypothesis of the PVM has been stated in Sec. I and is essen-

tially that the configurational energy can be expressed as

$$E = \sum_{i=1}^m V_i \alpha_i, \quad (2)$$

and that m , the maximum neighbor index in the summation, does not exceed the maximum neighbor separation contained in the cluster. For the cluster chosen here, m would correspond to fifth neighbors in a bcc lattice and fourth neighbors in a fcc lattice. The V_i 's are pairwise interaction parameters.

The final step is to maximize the PVM entropy measure

$$I(P_k) = - \sum_{k=1}^K W_k P_k \ln P_k \quad (3)$$

by variation of the P_k 's subject to the linear constraints given in Eq. (1). W_k is the multiplicity of the k th configuration and represents the number of configurations that are equivalent under cubic symmetry. Formally, the variation can be accomplished by the introduction of a Lagrange multiplier λ_j for each constraint, forming the augmented function $I'(P_k)$ given by

$$I'(P_k) = I(P_k) + \sum_{j=1}^J \lambda_j C_j(P_k), \quad (4a)$$

where

$$C_j(P_k) = \sum_{k=1}^K a_j^k P_k - b_j. \quad (4b)$$

The P_k 's can now be regarded as independent variables and the maximum of $I(P_k)$ is determined by the equations

$$\frac{\partial I(P_k)}{\partial P_k} = 0 = -W_k(1 + \ln P_k) + \sum_{j=1}^J \lambda_j a_j^k \quad (k=1, K). \quad (5)$$

Thus,

$$P_k = \exp\left(W_k^{-1} \sum_{j=1}^J \lambda_j a_j^k - 1\right). \quad (6)$$

The λ_j 's are now adjusted to satisfy the J linear constraints. This is accomplished by inserting this expression for the P_k 's into Eq. (1), giving J nonlinear equations in J unknowns (the λ_j 's). An iterative method for determining the P_k 's can then be used.

III. ATOMIC CONFIGURATION DISTRIBUTION

In this section the distributions of nearest-neighbor configurations are displayed for a number of alloys as determined by the PVM from available SRO data. In the case of fcc systems it is impractical to present the entire distribution since this would

involve over 300 distinct configurations. We have instead shown only clusters having enhancement factors (EF) greater than 1 and have shown only the first dozen or so. The EF is the ratio of a cluster's population in the SRO state to its population in an ideal random alloy of the same composition. The clusters are displayed in the order of their EF's whose magnitudes are given above each cluster. In addition, the percent of atoms in the lattice of a given kind that have that particular nearest-neighbor configuration (or one of its symmetrical equivalents) is given in parentheses beneath each cluster. The total percent of the distribution shown is indicated at the bottom of the table. A cluster can have a larger EF but a smaller lattice percentage than another cluster simply because the percentage of the latter cluster was higher in the completely random state. We have also used the convention of indicating the positions of only one kind of atom on the nearest-neighbor shell, the unlabeled positions being occupied by the other atom type.

β -CuZn

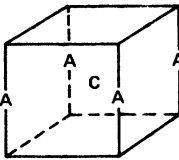
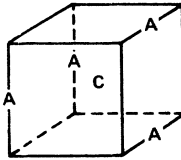
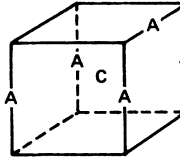
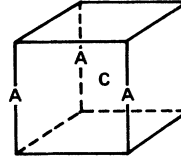
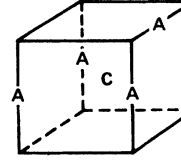
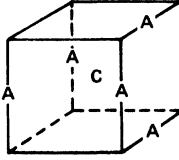
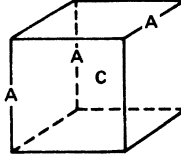
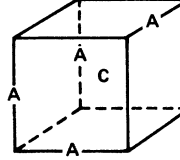
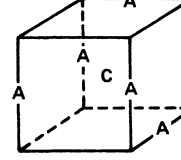
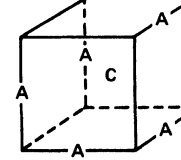
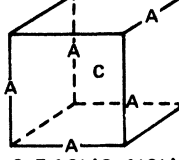
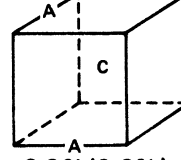
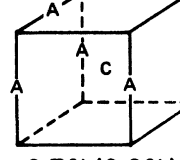
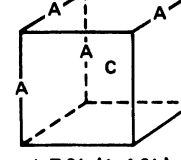
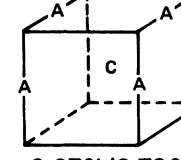
The complete nn spectrum of a Cu atom at 543 °C (10% above the ordering temperature) is shown in Table I for this bcc alloy as determined from the SRO parameters reported by Walker and Keating.⁷ Although the actual alloy contained 53.7-at. % Cu, the SRO parameters were determined on the basis of an equiatomic model and we have followed this assumption of a 50-50 alloy in our analysis. Thus the distribution for a Zn-center atom is obtained by interchanging Zn and Cu sites everywhere in Table I.

Qualitatively, the distribution is as one would expect. The most enhanced cluster is that representing the nearest-neighbor configuration in the perfectly ordered lattice, the next most enhanced is the "one-mistake" cluster, and the next three are the three possible "two-mistakes" clusters. A model of the SRO state based on the idea of perfectly ordered regions in a disordered matrix does not seem justified for this system. Since only 3% of the Cu (or Zn) atoms see a perfectly ordered nearest-neighbor environment, the volume fraction of such "microdomains" could be 3% at most.

Cu₃Au

Moss⁸ has measured the Warren SRO parameters at two temperatures above the ordering temperature in this system. Therefore, it is possible to determine the cluster distribution at these two temperatures and study the evolution of the SRO state as it approaches the long-range ordered (LRO) state. The distribution for Cu-centered clusters is given in Table II and that for Au-centered clusters in Table III. The numbers at the higher temperature (10% above T_c) are shown without parentheses and those for the lower temperature (3% above T_c) are

TABLE II. Nearest-neighbor spectrum of Cu atoms in Cu_3Au at $T=450^\circ\text{C}$ (405°C).

Cu_3Au $T=450^\circ\text{C}$ (405°C)				
$\alpha_1 = -.195(-.218)$ $\alpha_2 = +.215(+.286)$ $\alpha_3 = +.003(-.012)$ $\alpha_4 = +.077(+.122)$				
66.6 (112.8)  7.8% (13.2%)	28.8 (40.9)  6.8% (9.6%)	8.0 (7.2)  2.5% (2.2%)	6.8 (7.6)  9.6% (10.7%)	6.4 (7.2)  12.0% (13.5%)
5.2 (4.3)  1.6% (1.4%)	4.5 (4.5)  12.5% (12.9%)	4.2 (4.3)  7.9% (8.1%)	3.4 (2.4)  1.1% (0.75%)	3.4 (2.6)  1.1% (0.81%)
3.4 (2.6)  0.54% (0.41%)	2.9 (2.5)  2.8% (2.2%)	1.4 (1.4)  2.7% (2.6%)	1.4 (1.5)  1.3% (1.4%)	1.4 (1.5)  0.67% (0.70%)
TOTAL 71.6% (80.5%)				

in parentheses.

Several interesting aspects of the distribution are immediately apparent. There is a surprising degree of "order" in the nearest-neighbor environment even at the higher temperature. The Cu-centered perfect-order cluster is very highly enhanced

as compared to the comparable cluster in the Cu-Zn distribution at the same relative temperature. In fact, 34% of the Cu atoms and 64% of the Au atoms have one mistake or less in their nearest-neighbor shell at $T=1.10T_c$. These fractions increase to 42 and 77%, respectively, at $T=1.03T_c$.

TABLE III. Nearest-neighbor spectrum of Au atoms in Cu_3Au at $T=450^\circ\text{C}$ (405°C).

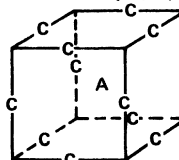
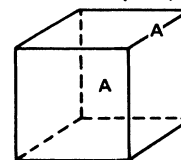
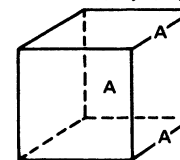
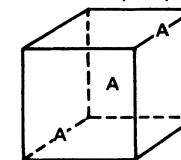
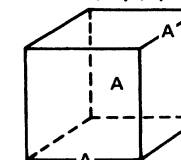
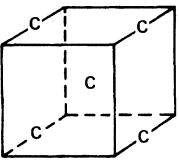
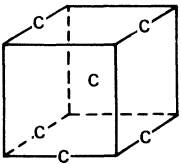
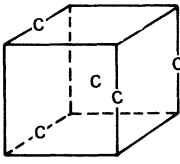
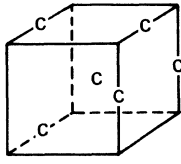
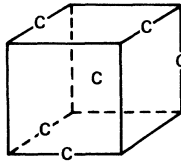
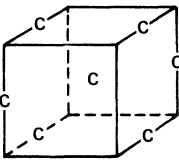
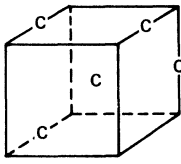
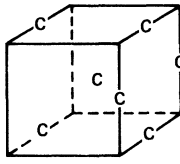
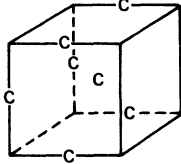
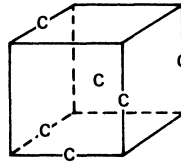
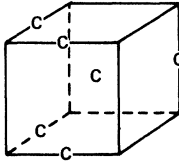
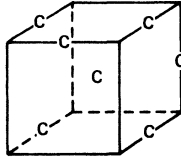
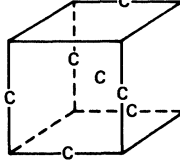
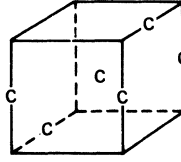
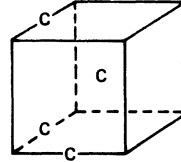
Cu_3Au $T=450^\circ\text{C}$ (405°C)				
$\alpha_1 = -.195(-.218)$ $\alpha_2 = +.215(+.286)$ $\alpha_3 = +.003(-.012)$ $\alpha_4 = +.077(+.122)$				
5.1 (6.4)  16.2% (20.3%)	3.8 (4.5)  48.3% (56.9%)	2.5 (2.0)  10.4% (8.4%)	1.6 (1.0)  3.4% (2.1%)	1.6 (1.1)  13.7% (9.3%)
TOTAL 92% (97%)				

TABLE IV. Nearest-neighbor spectrum of Cu atoms in CuAu at $T=425^\circ\text{C}$ ($T/T_c=1.025$).

CuAu $T = 425^\circ\text{C}$ ($T/T_c = 1.025$)				
$\alpha_1 = -.123$ $\alpha_2 = +.048$ $\alpha_3 = +.000$ $\alpha_4 = +.070$				
7.7  .57%	5.0  2.9%	4.4  .64%	3.7  2.2%	3.7  2.2%
3.7  1.1%	3.1  3.7%	2.8  .83%	2.8  .83%	2.8  1.7%
2.8  .83%	2.8  1.6%	2.8  1.6%	2.6  3.1%	2.4  2.8%
TOTAL 26.5 %				

The second most enhanced Cu-centered cluster is a particularly interesting type of mistake because it corresponds to the perfectly ordered environment of a different LRO arrangement variously referred to as the DO_{22} structure, the Ni_3V structure, or the Cu_3Au $M=1$ long-period superlattice. Moss and Clapp⁵ have previously demonstrated that the pair interactions in Cu_3Au are such that the normal $L1_2$ Cu_3Au structure is only slightly more favored energetically than the DO_{22} structure and this is undoubtedly the source of the "confusion" in the SRO state. It may be added that as one goes to the lower temperature although the other Cu-centered clusters either remain at the same lattice fraction or decrease, both the $L1_2$ and DO_{22} clusters increase appreciably so that this competition has a marked persistence and will appear in the LRO state as (001)-type antiphase boundaries.

CuAu

The SRO data of Roberts⁹ at $T=1.025T_c$ were used to generate the cluster distribution shown in Table IV. At this temperature the tendency to order into

the $L1_0$ structure is apparent but there is still a considerable degree of disorder present in the nearest-neighbor environment and the perfect-order cluster does not show nearly the same degree of dominance here as compared to the case of Cu_3Au .

Au₃Cu

In Tables V and VI the rather surprising distribution for Au_3Cu is given as derived from the SRO measurements of Batterman.¹⁰ It is normally thought that Au_3Cu orders in the $L1_2$ structure; but the most enhanced Cu-centered clusters are of the $L1_0$ CuAu type, and the fourth most enhanced cluster is even of the Cu_3Au type. The Au-centered cluster distribution is less paradoxical but it also shows a significant number of strongly enhanced clusters of the $L1_0$ CuAu type. If true, this would suggest that the ordering process in Au_3Cu is rather complex and implies that the transformation may actually be to an ordered $L1_0$ CuAu phase intermixed with a Au-rich phase rather than to a homogeneous $L1_2$ Au_3Cu phase. Since the superlattice reflections cannot distinguish between these two possibilities, the

fundamental reflections would have to be examined for appreciable broadening or splitting in the transformed state. The transformation is quite sluggish, however, so that it may require long times before the splitting of the fundamental spots is observable.

On the other hand, the SRO measurements in Au_3Cu are particularly difficult because of large-size-effect scattering and because of the difficulty in achieving equilibrium. Thus, the measured α 's may be inaccurate and if the errors were significant this would considerably distort the derived distributions.

Cu-14.5% Al

The α 's as determined by Houska and Averbach¹¹ from powder samples at -190°C were used to calculate the cluster distribution in Table VII. The SRO structure of this alloy has been of considerable interest ever since the radiation-damage experiments of Wechsler and Kernohan¹² showed that the electrical resistivity first decreases and then increases with increasing exposure time in a reactor. It was surmised that this anomalous behavior was

connected with the induced changes in the SRO of the alloy. Houska and Averbach also determined the α 's for an irradiated sample and found that all of the SRO parameters increased in magnitude relative to the normal sample, indicating a pronounced increase in the degree of the SRO. However, the value of α_1 that they report is 20% greater than the maximum theoretical limit for an alloy of this composition, which makes it impossible to generate the cluster distribution for the irradiated alloy. This error indicates that either the actual composition of the alloy was in excess of 17-at.% Al or the SRO diffuse scattering was not correctly separated from the other diffuse scattering contributions.

Borie and Sparks² afterwards performed a more detailed diffuse-scattering experiment in two planes of reciprocal space for single-crystal samples of Cu-16% Al alloys before and after irradiation. On the basis of their measurements, they suggested an interesting model for the SRO structure. They proposed that the Al atoms for the most part were grouped in tetrahedral clusters (the first cluster shown in Table VII) and that no Al nearest-neighbor

TABLE V. Nearest-neighbor spectrum of Cu atoms in Au_3Cu at $T=250^\circ\text{C}$ ($T/T_c=1.11$).

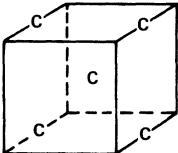
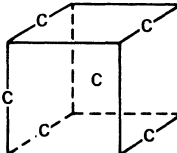
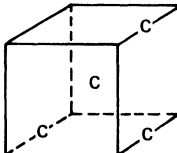
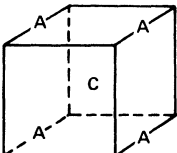
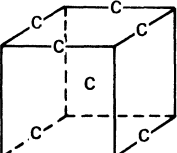
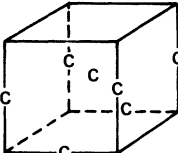
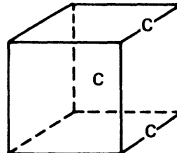
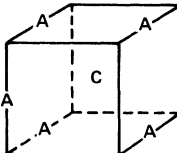
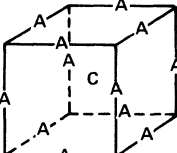
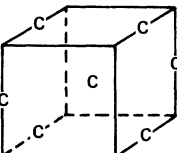
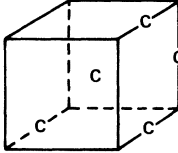
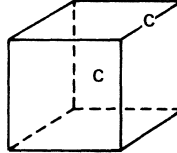
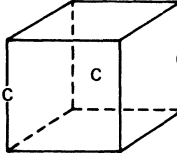
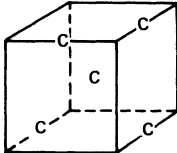
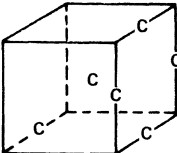
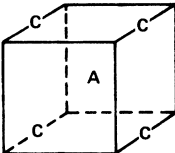
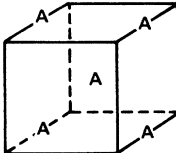
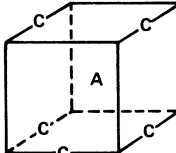
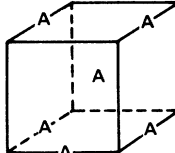
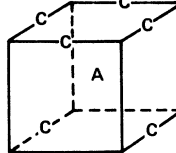
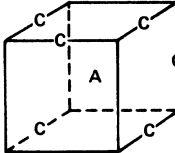
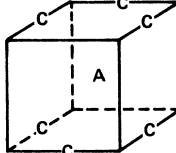
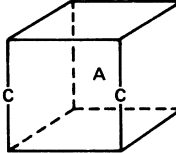
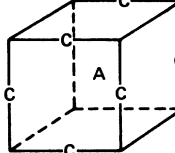
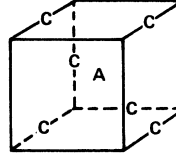
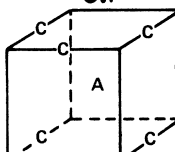
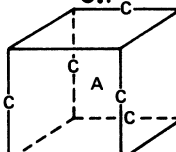
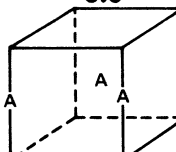
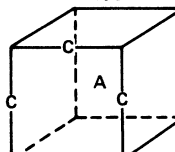
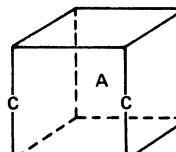
Au_3Cu $T=250^\circ\text{C}$ ($T/T_c=1.11$)				
$\alpha_1 = -.06$ $\alpha_2 = +.20$ $\alpha_3 = -.08$ $\alpha_4 = +.14$				
18.5  2.16%	5.1  1.59%	4.5  6.37%	3.3  .005%	2.8  .15%
2.8  .15%	2.3  9.55%	2.1  .08%	2.1  6.64%	1.9  .10%
1.7  3.21%	1.5  19.3%	1.5  3.14%	1.5  2.75%	1.3  .41%
TOTAL 55.6%				

TABLE VI. Nearest-neighbor spectrum of Au atoms in Au₃Cu at T=250°C (T/T_c=1.11).

Au₃Cu T = 250°C (T/T_c = 1.11)				
$\alpha_1 = -.06$ $\alpha_2 = +.20$ $\alpha_3 = -.08$ $\alpha_4 = +.14$				
27.9  3.27%	20.3  .03%	10.9  3.41%	9.3  .32%	8.7  .45%
8.7  .45%	5.7  .30%	4.8  6.81%	3.6  .75%	3.6  .75%
3.1  .32%	3.1  .32%	3.0  .006%	2.9  .89%	2.6  4.87%
TOTAL 23.0%				

pairs occurred. To further support their model, they observed that the β_1 -Cu₃Al metastable phase, which is an ordered DO₃ (BiF₃) structure and appears by quenching the bcc disordered β phase, may be described as an array of regular Al tetrahedra. Although the proposed Al groups in the fcc SRO phase are not regular tetrahedra (two sides are second-neighbor distances and four are third-neighbor distances), they are close to being so and the measured atomic displacements were of the right sign to improve the congruence.

Although their model is provocative, neither of their conjectures can be proven with certainty by their data and even within the framework of their model a considerable degree of freedom remains in the picture of the SRO structure arising from the various ways one can pack the tetrahedral groups.

Gehlen and Cohen³ took issue with the tetrahedral model on the basis of a computer simulation of the SRO structure that they generated using the SRO parameters of Houska and Averbach¹¹ (since the diffraction data of Borie and Sparks gives linear combinations of the α 's but not the α 's individually).

By visually scanning their computer-simulated patterns, they concluded that the dominant feature of the SRO structure consisted of linear chains of Al atoms in second-neighbor relationships and that isolated tetrahedral clusters were hardly ever observed.

Our cluster distribution in Table VII supports both models and shows that they are complementary rather than contradictory views of the SRO structure. On the one hand, by far the most enhanced cluster in the distribution is the tetrahedral group proposed by Borie and Sparks, so that the tendency of the system is quite clear. On the other hand, the lattice fraction of such clusters is still very small, so that they would not be a striking feature of an SRO configuration map. The tendency for Al atoms to avoid each other as nearest neighbors is also apparent since the only Al-centered cluster that is enhanced relative to the random state contains no Al atoms in its nearest-neighbor shell and constitutes 72% of the Al sites. This fraction undoubtedly approaches 100% in the irradiated samples.

Furthermore, the Al chains of Gehlen and Cohen will form a tetrahedral group at their point of closest approach if that separation is a second-neighbor distance and the chains are orthogonal. If they are parallel, they will form an array of square groups, which is the second most enhanced cluster in our distribution. Given the high density of chains necessary to account for the Al concentration and realizing that a nearest-neighbor approach of chains is nearly forbidden leads one to the conclusion that second-neighbor chain interactions will occur quite frequently in the Gehlen-Cohen scheme. Finally, one may observe that the Cu_3Al (DO_3) structure can be viewed as either a perfect array of second-neighbor Al chains separated by second-neighbor distances or as a perfect stacking of Al tetrahedra.



Recently Mozer, Keating, and Moss¹³ have determined the SRO parameters of this alloy at 550 °C from a diffuse-neutron-scattering measurement. The Cu-Ni phase diagram indicates a homogeneous

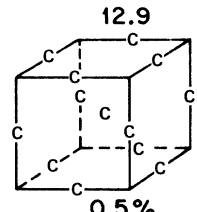
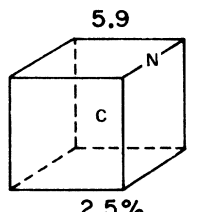
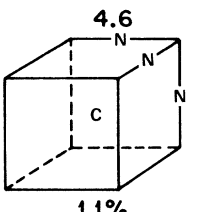
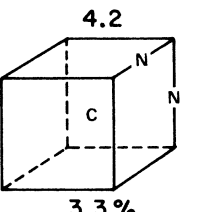
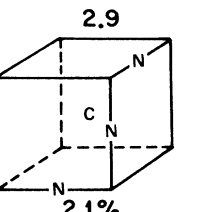
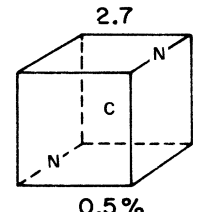
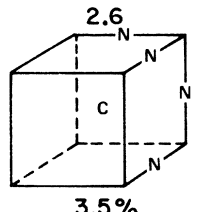
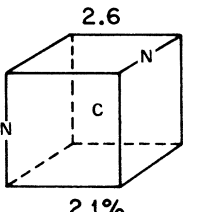
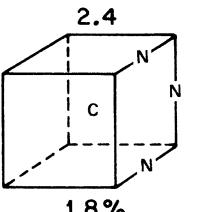
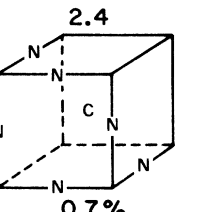
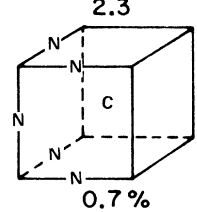
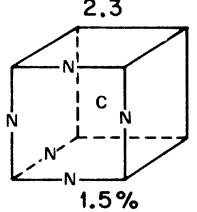
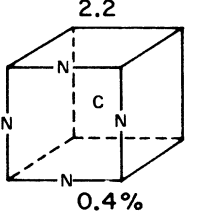
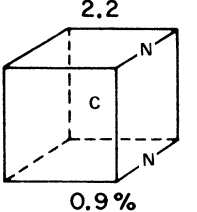
solid solution across the entire composition range but it is now generally agreed from thermodynamic data and SRO studies that Cu-Ni is potentially a clustering system with the predicted miscibility gap maximum at about 300 °C and 70-at.% Ni. Our calculated cluster distributions shown in Tables VIII and IX give further evidence for this tendency and provide some interesting information about the morphology of the pre-precipitation stage (actual precipitation does not occur presumably because of the low transformation temperature).

Although practically all of the enhanced clusters show that the central atom prefers to surround itself with its own kind, the other species appear to segregate on (111) planes. Over half the tabulated configurations can be classified in this manner if no more than one mistake is allowed, and this suggests that the clustering occurs as (111) platelets of each kind. This conjecture is supported by a prior study of Cohen,⁴ who made a computer simulation of the SRO state of this alloy and noticed these (111) platelets as a significant feature of his configurations.

TABLE VII. Nearest-neighbor spectrum in $\text{Cu}_{85.5}\text{Al}_{14.5}$.

$\text{Cu}_{85.5}\text{Al}_{14.5}$				
$\alpha_1 = -.137 \quad \alpha_2 = +.124 \quad \alpha_3 = +.096 \quad \alpha_4 = -.041$				
56 4.3%	22 0.8%	7.0 12.5%	6.5 3.9%	4.4 3.9%
3.9 0.1%	3.9 0.2%	3.7 2.2%	2.4 0.12%	2.3 1.4%
2.2 0.12%	1.8 9.4%	1.6 17.4%	1.5 0.08%	4.7 72%
TOTAL 56.4%				

TABLE VIII. Nearest-neighbor spectrum of Cu atoms in $\text{Cu}_{52}\text{Ni}_{48}$.

$\text{Cu}_{52}\text{Ni}_{48}$				
$\alpha_1 = +.121 \quad \alpha_2 = -.008 \quad \alpha_3 = +.011 \quad \alpha_4 = +.012$				
 12.9 0.5%	 5.9 2.5%	 4.6 1.1%	 4.2 3.3%	 2.9 2.1%
 2.7 0.5%	 2.6 3.5%	 2.6 2.1%	 2.4 1.8%	 2.4 0.7%
 2.3 0.7%	 2.3 1.5%	 2.2 0.4%	 2.2 0.9%	
TOTAL 21.6%				

In addition, Moss and Clapp⁵ have determined the strengths of first- and second-neighbor interactions in this alloy and found that the second-neighbor interactions (V_2) were negative (meaning that second neighbors prefer to be unlike) and from 50 to 65% as strong as the positive first-neighbor interaction (V_1). This places the alloy close to the limit of stability for phase separation on their lowest-energy structure diagram (Fig. 6 of Ref. 14) and adjacent to the energy region of stability for the $L1_1$ (CuPt-type) ordered structure. The $L1_1$ structure consists of alternate atomic (111) planes of each type and can be regarded as the atomic limit of the (111) platelet morphology.

Assuming that $V_2 = -\frac{2}{3}V_1$, one can calculate that the energy gained by replacing a Cu atom at the edge of a (111) Ni platelet by a Ni atom from the disordered matrix would be $2V_1$, as opposed to only V_1 for the binding energy of a site on the top or bottom surface of the platelet. This calculation assumes the average environment of an edge site would contain two Ni atoms of the platelet as nearest neighbors but no platelet atoms as second neighbors, whereas a surface site would have three Ni nearest

neighbors and three Ni second neighbors if the platelet were two or more atom layers thick. Thus one can expect from the energetics that in the nucleation phase the platelets would initially expand their diameter more rapidly than they would thicken, giving large thin regions of each kind of atom lying on (111) planes. We can then explain the structure of the SRO state as being simply the precursor of this predicted mode of growth.

A further prediction can be made that since the relative binding energies of surface and edge sites will be a very sensitive function of the ratio of V_2 to V_1 in this alloy, one can expect large changes in the precipitate morphology (if precipitation can be induced) and large changes in the SRO structure as a result of small variations in V_2/V_1 . Pressure or alloy additions should be sufficient to see these effects.

$\text{Au}_{60}\text{Pd}_{40}$

The Au-Pd binary diagram indicates a homogeneous solid solution at all compositions. However, the relative heats of formation show a maximum negative value at the 40-at. % Pd composition. The

largest anomalous changes in electrical resistivity and Hall constant after cold work and the greatest resistivity recovery upon annealing also occur at this composition. These facts suggest that a significant amount of SRO is present in this particular alloy and led Lin, Spruiell, and Williams⁶ to measure the SRO parameters by means of x-ray diffuse scattering. The measurements were made at room temperature on a single-crystal sample that had been slowly cooled from 1050 °C.

We have used the first four SRO parameters determined by Lin, Spruiell, and Williams to generate the Pd-centered cluster distribution shown in Table X and the Au-centered cluster distribution displayed in Table XI. The Pd-centered distribution is more easily analyzed and we shall confine our attention to it.

The most enhanced cluster is a tetrahedral arrangement of four Pd atoms about the central Pd atom. This is precisely the nearest-neighbor environment that an atom would have in the hypothetical AB analog of the DO_{22} structure proposed by Clapp and Moss,¹⁴ and shown below in Fig. 1. On

the basis of their analysis, Lin, Spruiell, and Williams have in fact suggested that this is the ordered structure that the system is tending toward and if so would be the first known example of this atomic arrangement in alloys. The ordered structure may also be described as an $M=1$ antiphase derivative of the $L1_0$ (CuAu) structure. This is perhaps significant because the second most enhanced cluster is the nearest-neighbor configuration of the $L1_0$ structure itself. All but two of the subsequent nine most enhanced clusters are single-defect relatives of one or the other of these first two clusters. Although the $M=1$ antiphase structure does not contain any $L1_0$ -type clusters, an $M=2$ (and all higher M) antiphase structure will have a mixture of these two cluster types. The $M=2$ structure is shown in Fig. 2. The proportion of $L1_0$ -type clusters increases as M increases and the $L1_0$ lattice may be regarded as the limit as M approaches infinity.

Although Lin, Spruiell, and Williams may be correct in their conjecture that the $M=1$ structure is the ultimate ordered state of this system, from

TABLE IX. Nearest-neighbor spectrum of Ni atoms in $Cu_{52}Ni_{48}$.

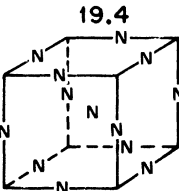
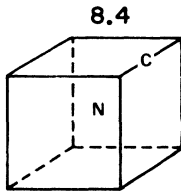
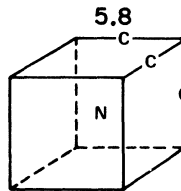
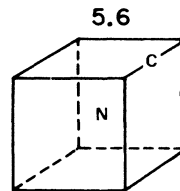
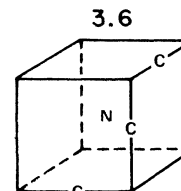
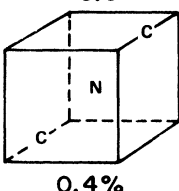
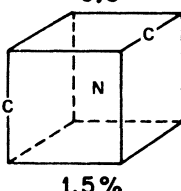
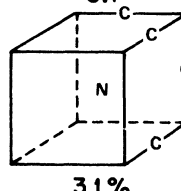
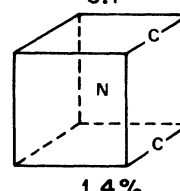
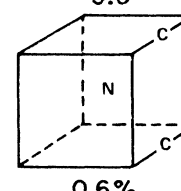
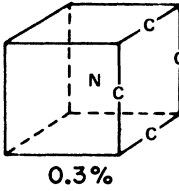
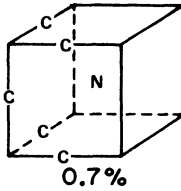
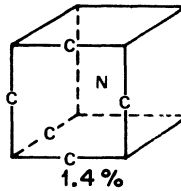
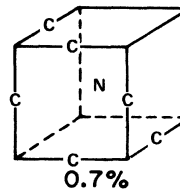
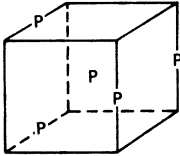
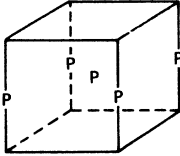
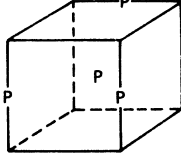
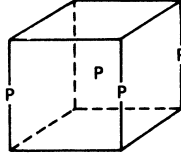
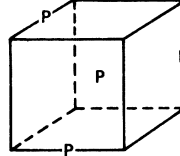
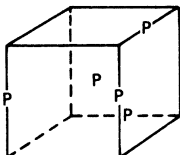
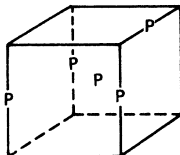
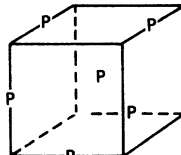
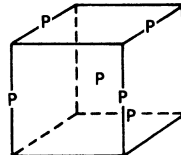
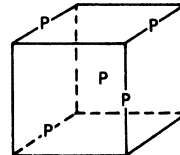
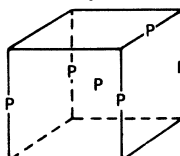
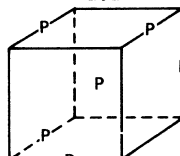
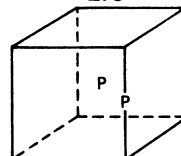
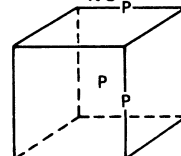
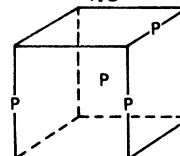
<u>$Cu_{52}Ni_{48}$</u>					
$\alpha_1 = +.121$		$\alpha_2 = -.008$		$\alpha_3 = +.011$	$\alpha_4 = +.012$
19.4  0.3%	8.4  1.6%	5.8  0.9%	5.6  2.4%	3.6  1.7%	
3.6  0.4%	3.5  1.5%	3.1  3.1%	3.1  1.4%	3.0  0.6%	
2.7  0.3%	2.6  0.7%	2.6  1.4%	2.6  0.7%		
TOTAL 17.0%					

TABLE X. Nearest-neighbor spectrum of Pd atoms in $\text{Au}_{60}\text{Pd}_{40}$.

$\text{Au}_{60}\text{Pd}_{40}$				
$\alpha_{110} = -.126$ $\alpha_{200} = +.061$ $\alpha_{211} = +.029$ $\alpha_{220} = -.033$				
6.4  1.65%	5.5  0.71%	3.6  5.54%	3.3  2.57%	3.3  1.65%
3.0  6.25%	2.8  5.80%	2.6  1.78%	2.6  0.89%	2.4  1.65%
2.2  1.56%	2.2  1.52%	2.0  2.34%	1.9  4.30%	1.8  5.70%
TOTAL 43.9%				

our cluster distribution it would appear that the $M=2$ structure is just as likely a candidate. An important observation made by the above investigators was that the diffuse SRO peak was actually a double peak lying at $1\frac{3}{8}0$ and $1\frac{5}{8}0$ in reciprocal space. This is not commensurate with the superlattice peak positions of any known structure. The superlattice positions for the $M=1$ structure would be at $1\frac{1}{2}0$ and those for the $M=2$ at $1\frac{3}{4}0$ and $1\frac{1}{4}0$.

The most likely explanation of this phenomenon is along the lines proposed by Moss¹⁵ and recently used by Hashimoto and Ogawa¹⁶ to explain the split diffuse peaks observed above T_c in Cu_3Au . Moss points out that, if the conduction-electron Fermi surface has a large flat region, this will produce a significant contribution to the interatomic ordering

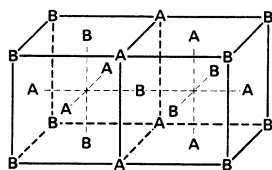


FIG. 1. $M=1$ antiphase derivative of the $L1_0$ (CuAu) structure.

energy in the form of a long-range oscillatory potential whose wavelength is related to the diameter of the Fermi "sphere" at the position of the flats. This oscillatory potential will produce composition fluctuations in the disordered phase of the same wavelength, which in general will not be compatible with the integral periods required of an ordered structure. The lowest-energy ordered structure will be the one having an oscillation in composition closest in wavelength to that of the conduction-electron oscillatory potential.

If this is the phenomenon that we are witnessing in the $\text{Au}_{60}\text{Pd}_{40}$ alloy, it offers some interesting information about the topology of the Fermi surface

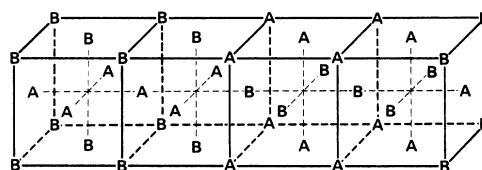
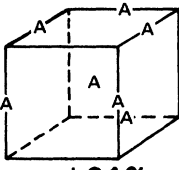
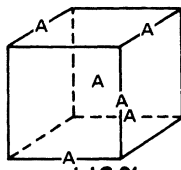
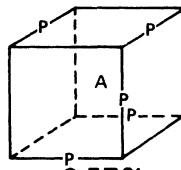
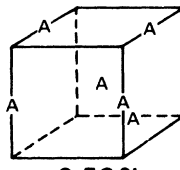
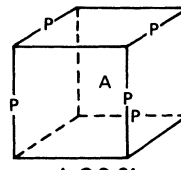
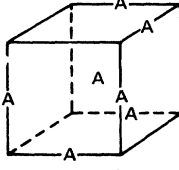
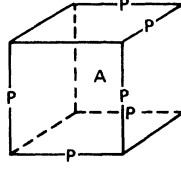
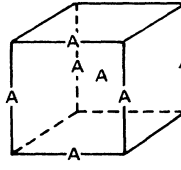
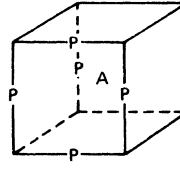
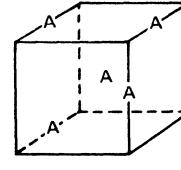
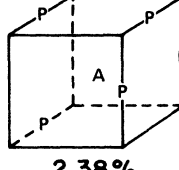
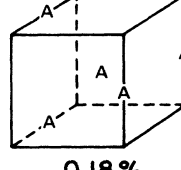
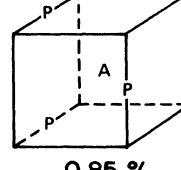
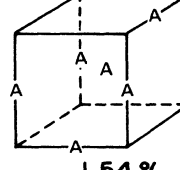
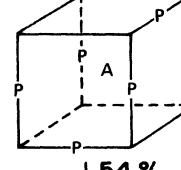


FIG. 2. $M=2$ antiphase derivative of the $L1_0$ structure.

TABLE XI. Nearest-neighbor spectrum of Au atoms in Au₆₀Pd₄₀.

<u>Au₆₀Pd₄₀</u>				
$\alpha_{110} = -.126$ $\alpha_{200} = +.061$ $\alpha_{211} = +.029$ $\alpha_{220} = -.033$				
4.2  1.94%	3.8  1.16%	3.7  2.57%	3.8  0.58%	3.7  1.29%
3.6  3.31%	3.6  3.31%	3.6  0.84%	3.6  0.84%	3.5  1.08%
3.5  2.38%	3.4  0.18%	3.3  0.85%	3.3  1.54%	3.3  1.54%
TOTAL 23.4%				

and partially explains the sluggish ordering behavior. Our conclusion is, however, that one still cannot decide whether the $M=1$ or the $M=2$ ordered structure will be the ultimate ground state.

APPENDIX: PVM TABLES FOR bcc AND fcc NEAREST-NEIGHBOR SHELL CLUSTERS

Following I, the configuration of a cluster is

TABLE XII. PVM parameters for bcc nearest-neighbor cluster. See Fig. 3 for site indices.

Index	Sites with $\sigma_i = -1$	Multiplicity W_k	Composition $W_k \langle \sigma \rangle_k$	Second neighbor $W_k C_k^2$	Third neighbor $W_k C_k^3$	Fifth neighbor $W_k C_k^5$
1($\bar{1}$)	...	1	+1(-1)	+1	+1	+1
2($\bar{2}$)	1	8	+6(-6)	+4	+4	+4
3($\bar{3}$)	1, 2	12	+6(-6)	+4	0	0
4($\bar{4}$)	1, 6	12	+6(-6)	0	+4	0
5($\bar{5}$)	1, 7	4	+2(-2)	0	0	+4
6($\bar{6}$)	1, 2, 5	24	+6(-6)	+4	-4	-12
7($\bar{7}$)	1, 2, 8	24	+6(-6)	-4	-4	+12
8($\bar{8}$)	1, 6, 8	8	+2(-2)	-4	+4	-4
9	1, 2, 5, 6	6	0	+2	-2	-6
10	1, 2, 5, 8	24	0	0	-8	0
11	1, 2, 5, 7	24	0	-8	0	0
12	1, 2, 3, 6	8	0	0	0	-8
13	1, 2, 7, 8	6	0	-2	-2	6
14	1, 3, 6, 8	2	0	-2	+2	-2

TABLE XIII. PVM parameters for fcc nearest-neighbor cluster. See Fig. 4 for site indices.

Index	Sites with $\sigma_i = -1$	Multiplicity W_k	Composition $W_k \langle \sigma \rangle_k$	First neighbor $W_k C_k^1$	Second neighbor $W_k C_k^2$	Third neighbor $W_k C_k^3$	Fourth neighbor $W_k C_k^4$
1($\bar{1}$)	...	1	+1(-1)	+1	+1	+1	+1
2($\bar{2}$)	6	12	+10(-10)	+8	+8	+8	+8
3($\bar{3}$)	6, 7	12	+8(-8)	+4	+8	+4	+4
4($\bar{4}$)	5, 7	6	+4(-4)	+2	+2	+2	+6
5($\bar{5}$)	6, 12	24	+16(-16)	+8	+8	+12	+8
6($\bar{6}$)	6, 11	24	+16(-16)	+12	+8	+8	+8
7($\bar{7}$)	5, 6, 7	12	+6(-6)	0	+8	0	+8
8($\bar{8}$)	5, 6, 12	24	+12(-12)	0	+8	+8	0
9($\bar{9}$)	1, 7, 9	8	+4(-4)	0	0	+4	0
10($\bar{10}$)	5, 6, 11	48	+24(-24)	+8	+16	+8	0
11($\bar{11}$)	4, 6, 11	48	+24(-24)	+8	0	+8	+32
12($\bar{12}$)	1, 5, 11	24	+12(-12)	+4	0	+8	0
13($\bar{13}$)	2, 6, 11	24	+12(-12)	+8	+8	0	0
14($\bar{14}$)	1, 6, 11	24	+12(-12)	+8	0	+4	0
15($\bar{15}$)	6, 10, 11	8	+4(-4)	+4	0	0	0
16($\bar{16}$)	5, 6, 7, 8	3	+1(-1)	-1	+3	-1	+3
17($\bar{17}$)	4, 6, 7, 9	6	+2(-2)	-2	+2	+2	-2
18($\bar{18}$)	5, 6, 8, 11	48	+16(-16)	-8	+16	0	+16
19($\bar{19}$)	3, 5, 6, 11	48	+16(-16)	-8	0	+16	-16
20($\bar{20}$)	1, 5, 10, 12	48	+16(-16)	0	+16	-8	+16
21($\bar{21}$)	1, 6, 7, 10	24	+8(-8)	0	+8	0	-8
22($\bar{22}$)	5, 6, 9, 11	12	+4(-4)	0	+4	0	-4
23($\bar{23}$)	1, 5, 7, 10	24	+8(-8)	0	0	0	+8
24($\bar{24}$)	4, 5, 6, 11	24	+8(-8)	0	0	0	+8
25($\bar{25}$)	1, 6, 9, 11	48	+16(-16)	0	0	+8	-16
26($\bar{26}$)	1, 5, 7, 12	12	+4(-4)	0	-4	0	+12
27($\bar{27}$)	1, 5, 7, 11	24	+8(-8)	0	-8	+4	+8
28($\bar{28}$)	2, 5, 7, 12	24	+8(-8)	0	-8	+4	+8
29($\bar{29}$)	2, 5, 9, 10	24	+8(-8)	+4	-8	0	+8
30($\bar{30}$)	1, 6, 11, 12	24	+8(-8)	+4	-8	0	+8
31($\bar{31}$)	1, 6, 7, 11	48	+16(-16)	+8	0	0	-16
32($\bar{32}$)	2, 6, 7, 11	6	+2(-2)	+2	+2	-2	-2
33($\bar{33}$)	1, 6, 10, 11	48	+16(-16)	+16	0	-8	-16
34($\bar{34}$)	5, 6, 7, 8, 11	24	+4(-4)	-8	+16	-8	+16
35($\bar{35}$)	4, 6, 7, 9, 11	24	+4(-4)	-8	+8	0	0
36($\bar{36}$)	1, 4, 7, 9, 11	24	+4(-4)	-8	0	+4	0
37($\bar{37}$)	1, 3, 6, 9, 11	24	+4(-4)	-8	0	+8	-16
38($\bar{38}$)	3, 5, 6, 9, 11	12	+2(-2)	-4	0	+4	-8
39($\bar{39}$)	2, 5, 6, 9, 11	48	+8(-8)	-8	+16	-8	0
40($\bar{40}$)	4, 5, 6, 7, 11	48	+8(-8)	-8	0	-8	+32
41($\bar{41}$)	1, 6, 7, 8, 11	48	+8(-8)	-8	0	0	0
42($\bar{42}$)	1, 3, 6, 11, 12	24	+4(-4)	-4	0	0	0

specified by an occupation number σ_i for each site which can have the value +1 or -1. σ_0 refers to the central site and σ_i (for $i = 1, z$) refers to the z

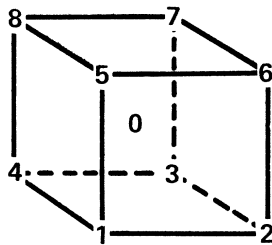


FIG. 3. Site numbering used for bcc clusters in Table XII.

sites in the nearest-neighbor shell around the central site. In the listing of cluster types (see Tables XII and XIII) we have specified only the shell sites having $\sigma_i = -1$ (the remainder of the shell sites are understood to have $\sigma_i = +1$). The various shell configurations are then labeled by the index k . It is not necessary to enumerate those clusters having negative occupation numbers on more than half of the shell sites. These configurations will be the complements of the tabulated clusters and can be generated from them by reversing the sign of σ_i on all shell sites. Each cluster k will thus have a complement which we denote by \bar{k} . Any summation over

TABLE XIII. (continued).

k	$\sigma_i = -1$	W_k	$W_k(\sigma)_k$	$W_k C_k^1$	$W_k C_k^2$	$W_k C_k^3$	$W_k C_k^4$
43(43)	1, 6, 7, 9, 11	48	+8(-8)	-8	0	+8	-32
44(44)	1, 6, 8, 9, 11	48	+8(-8)	-8	-16	+8	0
45(45)	1, 5, 6, 7, 10	24	+4(-4)	0	+8	-8	0
46(46)	1, 3, 6, 10, 11	48	+8(-8)	0	0	-8	0
47(47)	1, 5, 6, 7, 11	24	+4(-4)	0	0	-4	0
48(48)	5, 6, 9, 11, 12	24	+4(-4)	0	0	0	-16
49(49)	1, 6, 8, 10, 11	48	+8(-8)	0	-16	0	0
50(50)	1, 5, 6, 11, 12	48	+8(-8)	0	-16	0	0
51(51)	4, 6, 8, 10, 11	24	+4(-4)	0	-16	0	+16
52(52)	1, 4, 6, 11, 12	24	+4(-4)	0	-16	0	+16
53(53)	1, 6, 10, 11, 12	24	+4(-4)	+4	0	-8	0
54(54)	1, 6, 7, 10, 11	48	+8(-8)	+8	0	-8	-32
55(55)	1, 4, 6, 10, 11	48	+8(-8)	+8	-16	-8	0
56(56)	1, 2, 6, 10, 11	12	+2(-2)	+4	0	-4	-8
57(57)	1, 5, 6, 10, 11	24	+4(-4)	+8	0	-8	-16
58	1, 5, 6, 7, 8, 10	12	0	-4	+8	-4	+4
59	2, 4, 5, 6, 9, 11	12	0	-4	+8	-4	+4
60	4, 5, 6, 7, 8, 11	12	0	-4	+4	-4	+12
61	1, 5, 6, 7, 8, 11	24	0	-8	+8	-4	+8
62	2, 5, 6, 8, 9, 11	24	0	-8	+8	-4	+8
63	1, 3, 5, 6, 11, 12	48	0	-16	0	+8	-16
64	3, 5, 6, 7, 9, 11	48	0	-16	0	+8	-16
65	3, 5, 6, 9, 11, 12	24	0	-8	0	+8	-24
66	1, 3, 6, 8, 9, 11	12	0	-4	-4	+4	-4
67	1, 5, 6, 7, 10, 12	24	0	-4	+8	-8	+8
68	1, 3, 6, 10, 11, 12	24	0	-4	+8	-8	+8
69	1, 6, 7, 8, 10, 11	48	9	-8	0	0	-16
70	2, 5, 6, 9, 11, 12	48	0	-8	0	0	-16
71	1, 3, 6, 8, 10, 11	48	0	-8	-16	0	+16
72	1, 5, 6, 8, 11, 12	48	0	-8	-16	0	+16
73	1, 3, 6, 7, 10, 11	48	0	0	0	-8	-16
74	1, 5, 6, 8, 10, 11	48	0	0	0	-8	-16
75	1, 6, 7, 9, 10, 11	16	0	0	0	0	-16
76	1, 4, 6, 10, 11, 12	48	0	0	-16	-8	+16
77	1, 3, 4, 6, 10, 11	48	0	0	-16	-8	+16
78	1, 5, 6, 9, 11, 12	12	0	0	-4	0	-4
79	1, 2, 6, 8, 10, 11	12	0	0	-4	0	-4
80	1, 4, 6, 7, 10, 11	48	0	0	-16	0	-16
81	1, 4, 6, 8, 10, 11	48	0	0	-32	0	+16
82	3, 4, 6, 8, 10, 11	4	0	0	-4	0	+4
83	1, 4, 6, 8, 11, 12	4	0	0	-4	0	+4
84	1, 2, 6, 10, 11, 12	48	0	+8	0	-16	-16
85	1, 5, 6, 7, 10, 11	48	0	+8	0	-16	-16
86	1, 5, 6, 9, 10, 11	24	0	+8	0	-8	-24
87	1, 4, 5, 6, 10, 11	12	0	+4	-4	-4	-4

k henceforth implies summation over \bar{k} as well. The occupation of the central site is given by σ_0 and so the double index (σ_0, k) serves to specify the com-

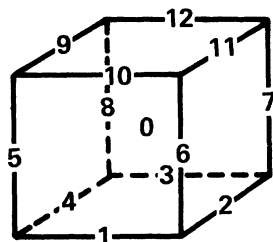


FIG. 4. Site numbering used for fcc clusters in Table XIII.

plete cluster configurations.

The multiplicity W_k is the number of symmetry partners that the k th shell configuration has. This is determined by counting the number of different configurations generated by applying the 48 symmetry operations of the cubic point group to the cluster. The less symmetric the cluster the more partners it will have, up to a maximum of 48. Because of the cubic symmetry of the lattice and the input data, these symmetric partners must all occur with equal probability and may thus be grouped together in the calculations. This considerably re-

duces the number of actual configurations to be dealt with.

$\langle \sigma \rangle_k$ is the average "composition" of the shell sites and is given by $\sum_{i=1}^n \sigma_i / z$. $\langle \sigma \rangle_k$ is the only tabulated quantity that changes for cluster complements (this being a change in sign) and is indicated by the entries in parentheses.

C_k^n is the average value in the cluster k of the occupation-number pair product $\sigma_i \sigma_j$ (where i, j are any two shell sites that are n th neighbors of each other) and may be determined by direct inspection of the cluster configuration. C_k^n is identical for the complement cluster. Because the coefficients of the PVM linear equations are the products $W_k C_k^n$, these are the quantities we have chosen to tabulate.

The linear constraint equations are as follows:

$$\sum_{\sigma_0} \sum_k W_k P(\sigma_0, k) = 1, \quad (\text{A1})$$

$$\sum_{\sigma_0} \sum_k \sigma_0 W_k P(\sigma_0, k) = c, \quad (\text{A2})$$

$$\sum_{\sigma_0} \sum_k \langle \sigma \rangle_k W_k P(\sigma_0, k) = c, \quad (\text{A3})$$

$$\sum_{\sigma_0} \sum_k \sigma_0 \langle \sigma \rangle_k W_k P(\sigma_0, k) = (1 - c^2) \alpha_1 + c^2, \quad (\text{A4})$$

$$\sum_{\sigma_0} \sum_k C_k^n W_k P(\sigma_0, k) = (1 - c^2) \alpha_n + c^2, \quad (\text{A5})$$

where c is the difference in atomic fraction of the two components and the α 's are the Warren SRO parameters.

If $c = 0$, then $P(\sigma_0, k) = P(\bar{\sigma}_0, \bar{k})$ and Eqs. (A2) and (A3) are redundant.

In Eq. (A5), n takes on the values (2, 3, and 5) for the bcc cluster and (1, 2, 3, and 4) for the fcc cluster.

The quantity to be maximized subject to these constraints is

$$I = - \sum_{\sigma_0} \sum_k W_k P(\sigma_0, k) \ln P(\sigma_0, k). \quad (\text{A6})$$

¹P. C. Clapp, *J. Phys. Chem. Solids* **30**, 2589 (1969).

²B. Borie and C. J. Sparks, Jr., *Acta Cryst.* **17**, 827 (1964).

³P. C. Gehlen and J. B. Cohen, *Phys. Rev.* **139**, A844 (1965).

⁴J. B. Cohen, *J. Mater. Sci.* **4**, 1012 (1969).

⁵S. C. Moss and P. C. Clapp, *Phys. Rev.* **171**, 764 (1968).

⁶W. Lin, J. E. Spruiell, and R. O. Williams, *J. Appl. Cryst.* (to be published).

⁷C. B. Walker and D. T. Keating, *Phys. Rev.* **130**, 1726 (1963). Walker and Keating actually measured quantities that are linear combinations of SRO parameters and the Zernike theory of ordering was used to extract the individual parameters. As such they will reflect the inaccuracies of Zernike's formula as well as any experi-

mental errors that may be present.

⁸S. C. Moss, *J. Appl. Phys.* **35**, 3547 (1964).

⁹B. W. Roberts, *Acta. Met.* **2**, 597 (1954).

¹⁰B. W. Batterman, *J. Appl. Phys.* **28**, 556 (1957).

¹¹C. R. Houska and B. L. Averbach, *J. Appl. Phys.* **30**, 1525 (1959).

¹²M. S. Wechsler and R. H. Kernohan, *Phys. Chem. Solids* **7**, 307 (1958).

¹³B. Mozer, D. T. Keating, and S. C. Moss, *Phys. Rev.* **175**, 868 (1968).

¹⁴P. C. Clapp and S. C. Moss, *Phys. Rev.* **171**, 754 (1968).

¹⁵S. C. Moss, *Phys. Rev. Letters* **22**, 1108 (1969).

¹⁶S. Hashimoto and S. Ogawa, *J. Phys. Soc. Japan* **29**, 710 (1970).